Chapter 14
Inelastic Behavior of High-Temperature Steel Under Cyclic Loading Conditions

Katharina Knape and Holm Altenbach

Abstract The paper at hand focusses on the constitutive equations to describe the inelastic material behavior of the high-temperature steel X20CrMoV12-1, widely known to be applied for power plant components. Therefore, the purpose is to model its response to a cyclic loading profile under which power plants operate the majority of time. An Armstrong–Frederick type model including a constitutive equation for the inelastic strain rate and an evolution equation for the backstress tensor is considered as basis for the application of the two-time-scale approach. The advantage will be a reduction in computational time while still being able to depict the complete material behavior. The finite element software ABAQUS is used to simulate the creep test as well as the cyclic loading regime of a bar at elevated temperatures.

Keywords Cyclic loading · Frederick–Armstrong model · Two-time-scale approach

14.1 Introduction

Power plants represent one of the most used power generating technologies of today. Their gas turbines are known to have a high performance density so the main purpose is to quickly close the gap between the power generally needed and the power provided through renewable resources. Due to this efficient kind of running, highly frequent start-ups and shut-downs of the system lead to complex mechanical and thermal loading conditions, mechanical loading in the sense of periodic stress and strain states and thermal loading meaning very high surrounding temperatures. Therefore, the high-temperature creep, a slow time-dependent deformation, is the main challenge faced by the material along with the cyclic loading conditions. The combination

K. Knape (✉) · H. Altenbach
Engineering Mechanics, Institute of Mechanics, Otto-von-Guericke-University Magdeburg, Universitätsplatz 2, 39104 Magdeburg, Germany
e-mail: katharina.knape@ovgu.de

H. Altenbach
e-mail: holm.altenbach@ovgu.de

H. Altenbach et al. (eds.), *Solid Mechanics, Theory of Elasticity and Creep*, Advanced Structured Materials 185, https://doi.org/10.1007/978-3-031-18564-9_14

of both greatly influences the component's life and may lead to failure earlier than expected. To prevent unforeseen events and investment costs, an understanding of the material's behavior and response to certain loading conditions through a reliable simulation is mandatory. In addition, it would be possible to predict the remaining lifetime or adapt the maintenance intervals more precisely.

These computations are very time-consuming. They need time integration procedures with very small time increments in the case of a cycle-by-cycle integration [1]. However, to omit these difficulties, calculation methods including time averaging approaches have been developed within the past years. They can be implemented into the finite element code with the aim of reducing computational time. This work focusses on applying the two-time-scale approach which is already known for the solution of differential equations of dynamical systems [1]. Now, it is also used to simulate inelastic material behavior in a numerically efficient way by differentiating between two time scales, a slow and a fast one, each of them accounting for certain processes [12]. Another technique has for example been suggested in [8], where a wavelet transformation-based multi-time scaling method depicts crystal plasticity. In addition, the cycle jumping method is described in [9] with the intention to model the material's response under periodic loading. Here, internal variables are calculated for as many loading cycles as needed until the integration scheme is stabilized. After that, the rate of change can be estimated for a determined number of cycles avoiding a further cycle-by-cycle integration.

The starting point to achieve the above is a constitutive model as used in [1, 4] which needs to include especially creep, as well as cyclic hardening and softening processes. It can either be a macroscale or microscale model, where for a macroscale-based model, the material parameters are calculated according to experimental data [4] by fitting the curves. With the intention of modeling the inelastic behavior of a realistic gas turbine or shaft, using a microscale model had the advantage of depicting the local deformation better but is numerically much more complex which is why in this paper, a macroscale-model is applied.

The widely known unified constitutive model was firstly used by [7], including an equation to describe the inelastic strain rate tensor and also considering an evolution equation for the backstress tensor. Chaboche picked up the concept and suggested a superposition of several backstress tensors with separate evolution equations [3]. The approach is limited though, since the number of material parameters and hence the complexity of the model is increasing and so is the numerical effort.

The mentioned constitutive models have been successfully applied to predict material behavior under various mechanical and thermal loading conditions, nevertheless, modeling cyclic loading remains challenging [1]. In Sect. 14.2, the equations according to the Armstrong–Frederick model are derived, followed by the explanation of the two-time-scale approach in the third section. The combination of the two is then implemented into the finite element software ABAQUS to model the response of the high-temperature steel X20CrMoV12-1 to small number of loading cycles.

14.2 Two-Time-Scale Technique

The basic idea of the two-time-scale method is the introduction of two different time scales T_0 and T_1 [2, 11, 14] with the aim of reducing the computational time when solving a system of differential equations of the form

$$\frac{\mathrm{d}\boldsymbol{x}}{\mathrm{d}t} = \boldsymbol{X}[t, \boldsymbol{x}(t)], \quad \boldsymbol{x}\,(0) = \boldsymbol{x}_0 \tag{14.1}$$

where $\boldsymbol{x}$ represents a set of unknown variables.

The first, slow time scale, is often also called 'natural time' or 'physical time' and it accounts for quasi-static loading and long-term behavior such as creep, see Eq. (14.2)

$$T_0\,(t) = t. \tag{14.2}$$

The second, fast or fine time scale, is described using a parameter μ with respect to the total time t_{end}

$$T_1\,(t) = \tau\,(t) = \frac{t}{\mu} \tag{14.3}$$

$$\mu = \frac{T}{t_{\mathrm{end}}} \ll 1. \tag{14.4}$$

The total time derivative then yields

$$\frac{\mathrm{d}}{\mathrm{d}t} = \frac{\delta}{\delta t} + \frac{1}{\mu}\frac{\delta}{\delta \tau}. \tag{14.5}$$

The result of this operation is a system of partial instead of ordinary differential equations which can be solved with an asymptotic series expansion [12] of the set of unknown variables $\boldsymbol{x}$ with respect to the factor μ

$$\boldsymbol{x}\,(t, \tau) = \boldsymbol{x}^{(0)}\,(t, \tau) + \mu \boldsymbol{x}^{(1)}\,(t, \tau) + \mu^2 \boldsymbol{x}^{(2)}\,(t, \tau) + \cdots \tag{14.6}$$

Also expanding the right-hand-side of the equation and inserting that into the total time derivative yields a set of differential equations. They can be sorted with respect to the order of μ

$$\mu^{(-1)} : \frac{\delta \boldsymbol{x}^{(0)}}{\delta \tau} = 0, \tag{14.7}$$

$$\mu^{(0)} : \frac{\delta \boldsymbol{x}^{(0)}}{\delta t} + \frac{\delta \boldsymbol{x}^{(1)}}{\delta \tau} = \boldsymbol{X}\left(t, \tau, \boldsymbol{x}^{(0)}\right), \tag{14.8}$$

$$\mu^{(1)} : \frac{\delta \boldsymbol{x}^{(1)}}{\delta t} + \frac{\delta \boldsymbol{x}^{(2)}}{\delta \tau} = \frac{\delta \boldsymbol{X}(t, \tau, \boldsymbol{x}^{(0)})}{\boldsymbol{\delta x}} \boldsymbol{x}^{(1)}. \tag{14.9}$$

In Eq. (14.7), it can be seen that the mean solution $\boldsymbol{x}^{(0)}$ is only a function of the slow time scale t.

Now, a time averaging operator has to be applied [1]

$$\langle f\,(t,\tau)\rangle = \frac{1}{T}\int_0^T f\,(t,\tau)\,\mathrm{d}\tau \tag{14.10}$$

resulting in the following system of differential equations to calculate the mean solution

$$\frac{\mathrm{d}\boldsymbol{x}^{(0)}}{\mathrm{d}t} = \overline{\boldsymbol{X}}\left(t,\boldsymbol{x}^{(0)}\right). \tag{14.11}$$

The solutions of higher orders of μ may also be calculated according to [14]. Nevertheless, this work focusses only on the mean solution, where the stress tensor takes the following form

$$\boldsymbol{\sigma}\,(t,\tau) = \boldsymbol{\sigma}^{(0)}\,(t) + \boldsymbol{\sigma}^{(1)}\,(\tau) \tag{14.12}$$

with the mean part $\boldsymbol{\sigma}^{(0)}\,(t)$ and the periodic part $\boldsymbol{\sigma}^{(1)}\,(\tau)$. The stress deviator and the backstress tensor were also decomposed the same way. The above mentioned method was tested in [1] and now needs to be applied to the material model described in Sect. 14.3.

14.3 Material Model

The material model is supposed to depict elastic and also inelastic behavior. Therefore, the Armstrong–Frederick type constitutive model is applied which includes a constitutive equation for the inelastic strain rate tensor and a nonlinear kinematic hardening rule for the backstress tensor. The material parameters required are already identified in [1, 4] for tempered martensitic steel.

14.3.1 Elastic Behavior

Under the assumption of small strains, the additive decomposition of the strain $\boldsymbol{\varepsilon}$ into an elastic $\boldsymbol{\varepsilon}^{\mathrm{el}}$ and inelastic $\boldsymbol{\varepsilon}^{\mathrm{in}}$ part is considered as the basis

$$\boldsymbol{\varepsilon} = \boldsymbol{\varepsilon}^{\mathrm{el}} + \boldsymbol{\varepsilon}^{\mathrm{in}}. \tag{14.13}$$

In order to define the elastic strain, Hooke's law is applied including the material parameters Young's modulus E, bulk modulus K, shear modulus G, and the Poisson's ratio ν as well as the stress tensor $\boldsymbol{\sigma}$. Here, tr means the trace and $\boldsymbol{I}$ denotes the unit tensor

$$\boldsymbol{\sigma} = K \operatorname{tr}\left(\boldsymbol{\varepsilon}^{\mathrm{el}}\right) \boldsymbol{I} + 2G\boldsymbol{\varepsilon}^{\mathrm{el}}, \tag{14.14}$$

with

$$K = \frac{E}{3(1-2\nu)}, \quad G = \frac{E}{2(1+\nu)}. \tag{14.15}$$

Taking into account the decomposition of the stress tensor into a spheric $\boldsymbol{\sigma}_m$ and a deviatoric part $\boldsymbol{\sigma}'$ yields

$$\sigma_m = \frac{1}{3}\operatorname{tr}(\boldsymbol{\sigma}), \tag{14.16}$$

$$\boldsymbol{\sigma}' = \boldsymbol{\sigma} - \sigma_m \boldsymbol{I}. \tag{14.17}$$

Within this paper, all deviators will be marked with a prime. The equation for the elastic strain can be derived as follows

$$\boldsymbol{\varepsilon}^{\mathrm{el}} = \frac{\sigma_m}{3K}\boldsymbol{I} + \frac{\boldsymbol{\sigma}'}{2G}. \tag{14.18}$$

14.3.2 Inelastic Behavior

Now, the inelastic strain $\varepsilon^{\mathrm{in}}$ needs to be determined. It is known that in the case of creep behavior the inelastic strain rate has to be a function of the potential depending on the three invariants J_1, J_2, and J_3 of the stress tensor and can therefore be written as

$$\dot{\boldsymbol{\varepsilon}}^{\mathrm{in}} = \frac{\delta\psi(J_1(\boldsymbol{\sigma}'), J_2(\boldsymbol{\sigma}'), J_3(\boldsymbol{\sigma}'))}{\delta\boldsymbol{\sigma}'}. \tag{14.19}$$

Since there is no significant change of volume due to the inelastic deformation, only the stress deviator is considered. The influence of the first and third invariants may be neglected, since for a deviator, the first invariant is equal to zero [4]. The third invariant accounts only for so-called second-order effects in the material belonging to the tensorial-nonlinear behavior [13]. So in the simplest case, the inelastic strain is only dependent on the second invariant of the stress deviator

$$\dot{\boldsymbol{\varepsilon}}^{\mathrm{in}} = \frac{\delta\psi(J_2(\boldsymbol{\sigma}'))}{\delta\boldsymbol{\sigma}'} \tag{14.20}$$

which yields

$$\dot{\boldsymbol{\varepsilon}}^{\mathrm{in}} = \frac{3}{2}\,\dot{\varepsilon}^{\mathrm{in}}_{\mathrm{vM}}\frac{\boldsymbol{\sigma}'}{\sigma_{\mathrm{vM}}} \tag{14.21}$$

with the von Mises stress σ_{vM}

$$\sigma_{\mathrm{vM}} = \sqrt{\frac{3}{2}\boldsymbol{\sigma}' : \boldsymbol{\sigma}'} \tag{14.22}$$

and the von Mises inelastic strain rate $\dot{\varepsilon}^{\mathrm{in}}_{\mathrm{vM}}$

$$\dot{\varepsilon}^{\mathrm{in}}_{\mathrm{vM}} = \sqrt{\frac{2}{3}\dot{\boldsymbol{\varepsilon}}^{\mathrm{in}} : \dot{\boldsymbol{\varepsilon}}^{\mathrm{in}}}. \tag{14.23}$$

Note that $\dot{\boldsymbol{\varepsilon}}^{\mathrm{in}}$ is a deviator.

Power plant components are not only subjected to mechanical but also very high thermal loading. To account for the temperature dependency of the inelastic strain rate, a separation ansatz is applied as can be seen in Eq. (14.24). It includes the stress response function f_σ and a temperature response function $R(\vartheta)$ depending on the absolute temperature ϑ

$$\dot{\varepsilon}^{\mathrm{in}} = f_\sigma(\tilde{\sigma}_{\mathrm{vM}})R(\vartheta). \tag{14.24}$$

These functions are identified by fitting experimental data of the material under monotonic loading conditions.

Furthermore, the stress deviator is decomposed into an active $\widetilde{\boldsymbol{\sigma}}$ and a backstress part $\boldsymbol{\beta}$. The tensor's active part will now be denoted by $\tilde{(...)}$

$$\boldsymbol{\beta} = \boldsymbol{\sigma}' - \widetilde{\boldsymbol{\sigma}}. \tag{14.25}$$

To mathematically describe the backstress tensor, an Armstrong–Frederick type backstress [1] with two material parameters B_i is chosen

$$\dot{\boldsymbol{\beta}} = B_1\dot{\boldsymbol{\varepsilon}}^{\mathrm{in}} - B_2\,\dot{\varepsilon}^{\mathrm{in}}_{\mathrm{vM}}\boldsymbol{\beta}. \tag{14.26}$$

The term containing the von Mises inelastic strain rate is called dynamic recovery term and is known to improve the numerical results [4]. In order to also be able to capture cyclic behavior, the superposition of backstresses according to [3] is used where each of the backstresses has its own evolution equation described in Eq. (14.28)

$$\boldsymbol{\beta} = \sum_{i=1}^{n}\boldsymbol{\beta}_i\ , \tag{14.27}$$

$$\dot{\boldsymbol{\beta}}_i = B_1\dot{\boldsymbol{\varepsilon}}^{\mathrm{in}} - B_2\,\dot{\varepsilon}^{\mathrm{in}}_{\mathrm{vM}}\boldsymbol{\beta}_i. \tag{14.28}$$

This approach is limited by the ability of identifying the material parameters needed.

14.3.3 Application of the Two-Time-Scale Approach

The backstress tensor for isothermal loading conditions in particular is shown in [1]

$$\dot{\boldsymbol{\beta}} = \frac{2}{3} R\left(\vartheta\right) \left[\dot{\varepsilon}^{\text{in}} - \frac{3}{2} \dot{\varepsilon}_{\text{vM}} \frac{\boldsymbol{\beta}}{h\left(\sigma_{\text{vM}}, \vartheta\right)} \right]. \tag{14.29}$$

Including the before mentioned decomposition (Eq. 14.12) of the variables leads to the set of constitutive equations given in Eqs. (14.30)–(14.33) with $C_h(\vartheta) = 8.84$ [1]

$$\dot{\boldsymbol{\varepsilon}}^{\text{in}(0)} = \frac{3}{2} R(\vartheta) \left\langle \frac{f_\sigma\left(\widetilde{\sigma}_{\text{vM}}\right)}{\widetilde{\sigma}_{\text{vM}}} \left(\boldsymbol{\sigma}'^{(0)} - \boldsymbol{\beta}^{(0)} + \boldsymbol{\sigma}'^{(1)}\right) \right\rangle \tag{14.30}$$

$$\dot{\boldsymbol{\beta}}^{(0)} = \frac{2}{3} C_h\left(\vartheta\right) \left(\dot{\boldsymbol{\varepsilon}}^{\text{in}(0)} - \frac{3}{2} \boldsymbol{\beta}^{(0)} \left\langle \frac{\dot{\varepsilon}_{\text{vM}}^{(0)}}{h\left(\widetilde{\sigma}_{\text{vM}}, \vartheta\right)} \right\rangle \right) \tag{14.31}$$

and

$$\widetilde{\sigma}_{\text{vM}} = \sqrt{\frac{3}{2} \text{tr}\left(\boldsymbol{\sigma}'^{(0)} - \boldsymbol{\beta}^{(0)} + \boldsymbol{\sigma}'(1)\right)^2} \tag{14.32}$$

$$\dot{\varepsilon}_{\text{vM}}^{(0)} = \sqrt{\frac{2}{3} \text{tr}\left(\dot{\boldsymbol{\varepsilon}}^{\text{in}(0)^2}\right)}. \tag{14.33}$$

The response functions for high-temperature steel were developed in [10] with the parameters a_0, α, B, and H_* which should be estimated experimentally

$$R(\vartheta) = a_0 e^{-\frac{\alpha}{\vartheta}}, \; f(\sigma) = \sinh B\sigma, \; h(|\sigma|, \vartheta) = H_* |\sigma|. \tag{14.34}$$

14.4 Simulation of the Material Behavior

The simulation of the inelastic material behavior is done using the finite element program ABAQUS. An user-defined subroutine implements the specific material properties of X20CrMoV12-1 [5, 6]. First investigations are done modeling only one single element, now a bar, clamped on one side, is considered as shown in Fig. 14.1.

Fig. 14.1 Schematic model of the bar

14.4.1 Cyclic Loading Condition

Referring to the application of high-temperature steels such as X20CrMoV12-1 in power plants, these components are mostly subjected to cyclic loading. Therefore, a combined uniaxial load of the form described in Eq. (14.12) is considered. In this paper, the stress profile is assumed to be of rectangular shape, as can be seen in Fig. 14.2 with the mean stress $\sigma_m > 0$ and the amplitude $0 < \sigma_a < \sigma_m$. In [10], the material parameters for a surrounding temperature of $\vartheta = 835$ K can be found

$$\begin{aligned} a_0 &= 4.64 \times 10^{23}\ \frac{1}{\mathrm{h}},\ \alpha = 6.12 \times 10^{4}\ \frac{1}{\mathrm{K}},\ C_h = 8.84, \\ B &= 7.74 \times 10^{-2}\ \frac{1}{\mathrm{MPa}},\ H_* = 0.46. \end{aligned} \tag{14.35}$$

The loading parameters are chosen as follows

$$\sigma_m = 200\ \mathrm{MPa},\ \sigma_a = 10\ \mathrm{MPa} \tag{14.36}$$

for a total simulation time of $t_{\mathrm{end}} = 60$ min.

14.4.2 Results of the Finite Element Simulation

The results of the simulation including the material parameters described before can be seen in Fig. 14.3. The surrounding temperature was set to 873 K which tends to be the operating temperature of a power plant. Additionally, the initial condition of the inelastic and elastic strain being zero was chosen. Figure 14.4 shows the same loading profile but with the mean stress measuring 100 MPa, exactly half of the first simulation. The comparison between both of them can be seen in Fig. 14.5. If the mean stress is increased further from 100 to 200 MPa by steps of 20 MPa, the curve is shifted upward as shown in Fig. 14.6.

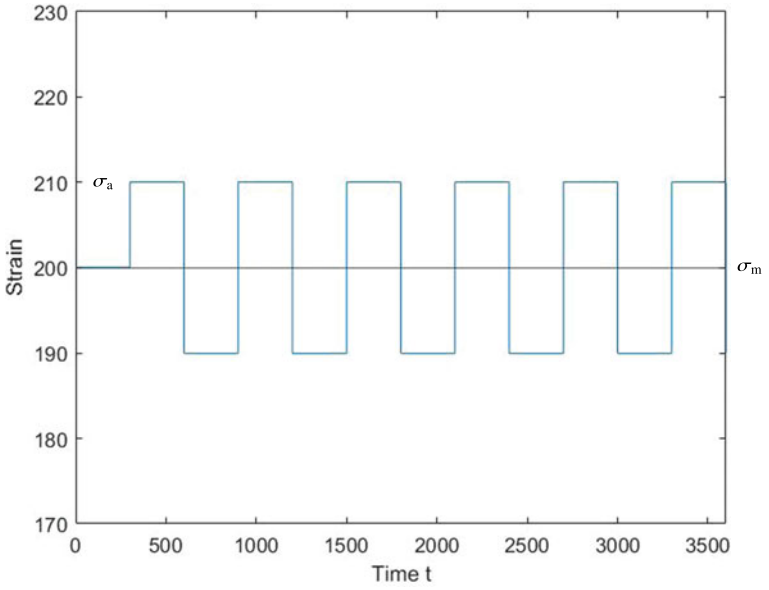

Fig. 14.2 Cyclic loading profile

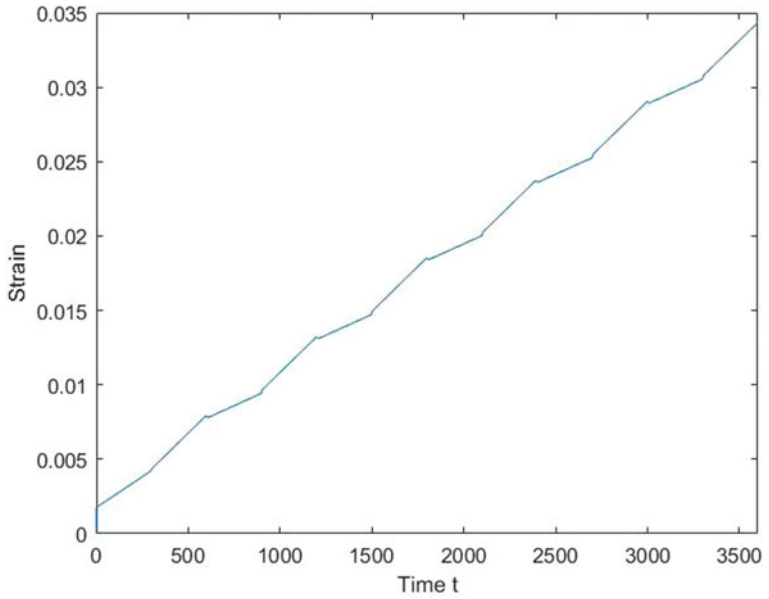

Fig. 14.3 Strain versus time for the given cyclic stress profile

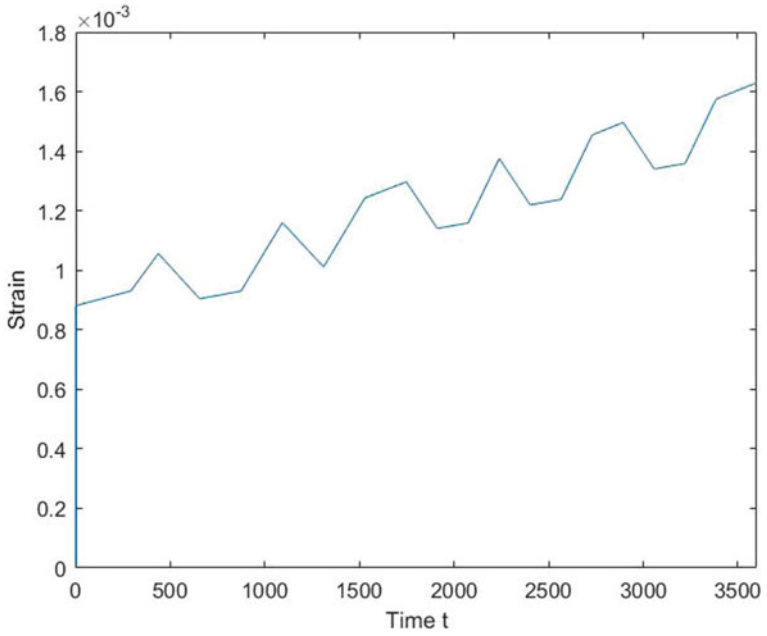

Fig. 14.4 Strain versus time with a mean stress of $\sigma_m = 100$ MPa

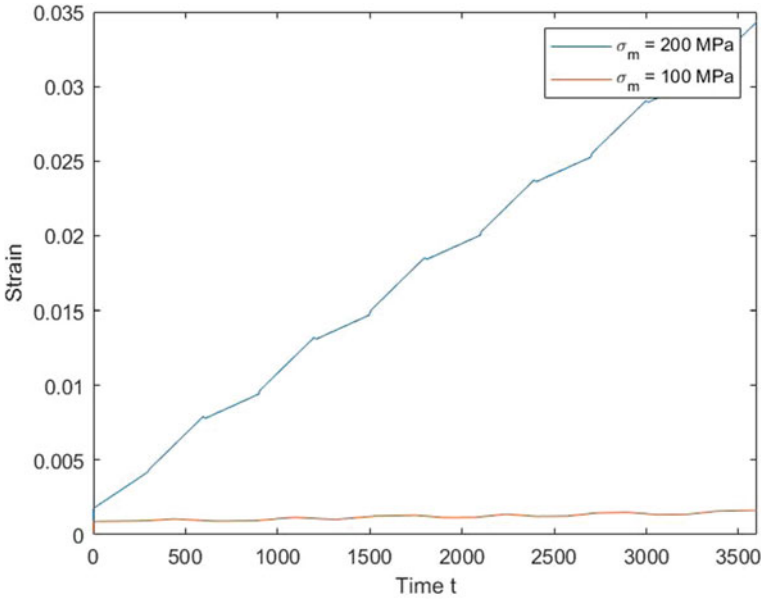

Fig. 14.5 Comparison of the strain versus time curves with the different mean stresses

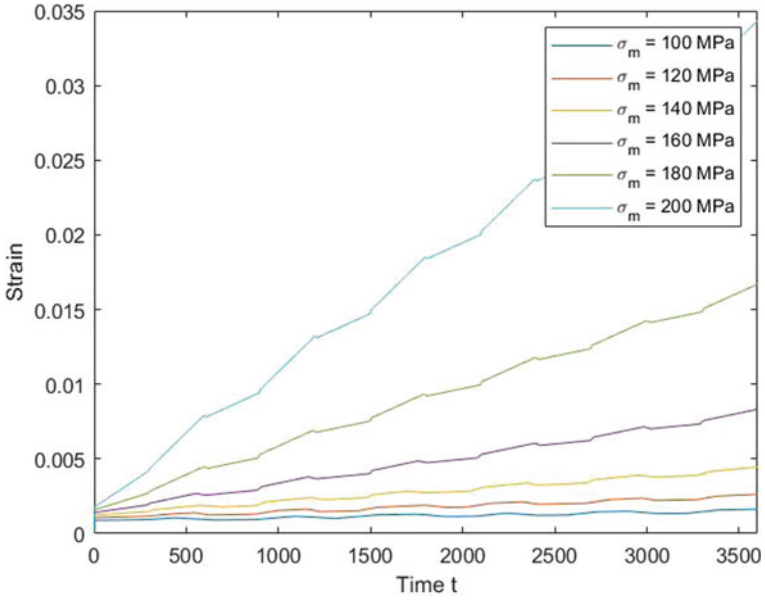

Fig. 14.6 Strain versus time for the given cyclic stress profile

14.5 Conclusion

The aim of this paper was to examine the inelastic material response of high-temperature steel to a cyclic loading profile as it can be found in several real-life applications such as power plants. The widely known Armstrong–Frederick constitutive model was used to model the material behavior. Applying the two-time-scale approach to the derived equations results in a reduction of the computational time needed when the finite element simulation using ABAQUS is carried out.

The applied material model includes the influence of the cyclic loading parameters such as mean stress and stress amplitude depending on the two time scales. The graph showing the strain with respect to time shifts as expected when the magnitude of the load is decreased.

Current and future investigations focus on deriving the constitutive equations and applying the two-time-scale approach also for the inelastic behavior due to thermal cyclic loading conditions or a combination of thermo-mechanical loading.

References

1. Altenbach, H., Breslasky, D., Naumenko, K., Tatarinova, O.: Two-time-scales and time-averaging approaches for the analysis of cyclic creep based on Armstrong-Frederick type constitutive model. J. Mech. Eng. Sci. **233**, 1690–1700 (2018)
2. Bensoussan, A., Lions, J.-L., Papanicolaou, G.: Asymptotic Analysis for Periodic Structures. North Holland Pub. Co., Amsterdam; American Mathematical Society, New York (1978)
3. Chaboche, J.L.: Constitutive equations for cyclic plasticity and cyclic viscoplasticity. Int. J. Plast. **5**, 247–302 (1989)
4. Eisenträger, J.: A framework for modeling the mechanical behavior of tempered martensitic steels at high temperatures. PhD thesis, Otto-von-Guericke-Universität Magdeburg (2018)
5. Eisenträger, J., Naumenko, K., Altenbach, H.: Numerical implementation of a phase mixture model for rate-dependent inelasticity of tempered martensitic steels. Acta Mech. **229**, 3051–3068 (2018)
6. Eisenträger, J., Zhang, J., Song, C., Eisenträger, S.: An SBFEM approach for rate-dependent inelasticity with application to image-based analysis. Int. J. Mech. Sci. **182**, 105778 (2020)
7. Frederick, C.O., Armstrong, P.J.: A mathematical representation of the multi axial Bauschinger effect. CEGB Report RD/B/N 731, Central Electricity Generating Board. The Report is Reproduced as a Paper: 2007 Materials at High Temperatures, vol. 24, pp. 1–26 (1966)
8. Joseph, D.S., Chakraborty, P., Ghosh, S.: Wavelet transformation based multi-time scaling method for crystal plasticity FE simulations under cyclic loading. Comput. Methods Appl. Mech. Eng. **199**, 2177–2194 (2010)
9. Labergere, C., Saanouni, K., Sun, Z.D., Dhifallah, M.H., Li, Y., Duval, Y.L.: Prediction of low cycle fatigue life using cycles jumping integration scheme. Appl. Mech. Mater. **784**, 308–316 (2015)
10. Naumenko, K., Altenbach, H., Kutschke, A.: A combined model for hardening, softening, and damage processes in advanced heat resistant steels at elevated temperature. Int. J. Damage Mech. **20**, 578–597 (2011)
11. Nayfeh, A.H.: Introduction to Perturbation Techniques. Wiley-VCH, New York (1993)
12. Oskay, C., Fish, J.: Fatigue life prediction using 2-scale temporal asymptotic homogenization. Int. J. Numer. Methods Eng. **61**, 326–359 (2004)
13. Reiner, M., Abir, D.: Second Order Effects in Elasticity, Plasticity and Fluid Dynamics. Pergamon Press, Oxford (1964)
14. Sanders, J.A., Verhulst, F.: Averaging Methods in Nonlinear Dynamical Systems. Springer, New York (1985)